Buckling of a Circular Plate Resting Over an Elastic Foundation in Simple Shear Flow

Haoxiang Luo[1]
Department of Mechanical Engineering,
Vanderbilt University,
VU Station B 351592,
2301 Vanderbilt Pl,
Nashville, TN 37235-1592
e-mail: haoxiang.luo@vanderbilt.edu

C. Pozrikidis
Department of Mechanical and Aerospace Engineering,
University of California, San Diego,
La Jolla, CA 92093-0411

The elastic instability of a circular plate adhering to an elastic foundation modeling the exposed surface of a biological cell resting on the cell interior is considered. Plate buckling occurs under the action of a uniform body force due to an overpassing simple shear flow distributed over the plate cross section. The problem is formulated in terms of the linear von Kármán plate bending equation incorporating the body force and the elastic foundation spring constant, subject to clamped boundary conditions around the rim. The coupling of the plate to the substrate delays the onset of the buckling instability and may have a strong effect on the shape of the bending eigenmodes. Contrary to the case of uniform compression, as the shear stress of the overpassing shear flow increases, the plate always first buckles in the left-to-right symmetric mode.
[DOI: 10.1115/1.2937137]

Keywords: membrane wrinkling, winkler foundation, elastic instability, plate buckling, shear flow

1 Introduction

The elastic instability of beams and plates is of prime interest in mainstream engineering design where critical conditions for structural stability under a compressive edge load must be established. Analytical and numerical results are available in the classical mechanics and applied engineering literature for plates with various shapes and a variety of boundary conditions (e.g., see Refs. [1,2]). The buckling of beams and plates with rectangular and circular shapes adhering to an elastic foundation has been studied by analytical and numerical methods on several occasions. Recently, Wang [3] studied the nonaxisymmetric buckling of a Kirchhoff plate resting on a Winkler foundation, provided analytical solutions for the eigenfunctions, and identified the most unstable buckling mode.

In this paper, we consider the buckling of a plate resting on an elastic foundation under a distributed tangential body force. Motivation is provided by the possible buckling of the membrane of an endothelium or cultured cell adhering to a substrate under the influence of an overpassing shear flow. In the physical model, the membrane is a composite medium consisting of the bilayer and the cytoskeleton, tethered to the cell interior by macromolecules that resist deflection and introduce an elastic response. Fung and Liu [4] discussed the mechanics of the endothelium and proposed that the main effect of an overpassing shear flow is to generate tensions over the exposed part of the cell membrane, while the cell interior is virtually unstressed. In an idealized depiction, the exposed membrane is a thin elastic patch anchored around its edges on the endothelium wall and connected to the basal lamina by sidewalls. In the present model, we also account for the elastic coupling between the cell membrane and the cell interior. Luo and Pozrikidis [5] considered the problem in the absence of the elastic substrate and uncovered the spectrum of eigenvalues corresponding to symmetric and antisymmetric deflection modes. Subsequently, Luo and Pozrikidis [6] investigated the effect of prestress with the goal of evaluating the buckling of the rotating capsule membrane. The present formulation extends these analyses and delineates critical conditions in the particular context of membrane mechanics and in the broader context of elastic stability pertinent to flow-structure interaction.

2 Theoretical Model

We consider a circular membrane patch modeled as an elastic plate flush mounted on a plane wall with the edge clamped around the rim (Fig. 1.) The upper surface of the membrane is exposed to an overpassing shear flow along the x axis with velocity $u_x = Gz$, where G is the shear rate and the z axis is normal to the wall. The lower surface of the membrane adheres to an elastic medium modeled as an elastic foundation.

The shear flow imparts to the upper surface of the membrane a uniform hydrodynamic shear stress, $\tau = \mu G$, where μ is the fluid viscosity. In the context of thin-shell theory for a zero thickness membrane, the shear stress can be smeared from the upper surface into the cross section of the membrane. When this is done, the shear stress effectively amounts to an in-plane body force uniformly distributed over the cross section with components

$$b_x = \frac{\tau}{h} = \frac{\mu G}{h}, \quad b_y = 0 \tag{1}$$

where h is the membrane thickness.

We assume that the in-plane stresses developing due to the in-plane deformation in the absence of buckling, σ_{ij}, are related to the in-plane strains ϵ_{ij} by the linear constitutive equation

$$\begin{bmatrix} \sigma_{xx} \\ \sigma_{yy} \\ \sigma_{xy} \end{bmatrix} = \frac{E}{1-\nu^2} \begin{bmatrix} 1 & \nu & 0 \\ \nu & 1 & 0 \\ 0 & 0 & 1-\nu \end{bmatrix} \cdot \begin{bmatrix} \epsilon_{xx} \\ \epsilon_{yy} \\ \epsilon_{xy} \end{bmatrix} \tag{2}$$

where

$$\epsilon_{kl} = \frac{1}{2}\left(\frac{\partial v_k}{\partial x_l} + \frac{\partial v_l}{\partial x_k} \right) \tag{3}$$

(v_x, v_y) is the tangential displacement of membrane point particles in the xy plane, E is the membrane modulus of elasticity, and ν is the Poisson ratio. Force equilibrium requires the differential balances

[1]Corresponding author.

Contributed by the Applied Mechanics Division of ASME for publication in the JOURNAL OF APPLIED MECHANICS. Manuscript received July 3, 2007; final manuscript received March 27, 2008; published online July 15, 2008. Review conducted by Krishna Garikipati.

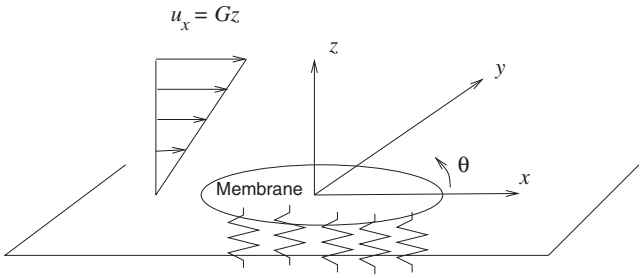

Fig. 1 Shear flow past a membrane patch modeled as an elastic plate flush mounted on a plane wall. The lateral deformation of the membrane is resisted by an elastic material supporting the membrane from underneath.

$$\frac{\partial \sigma_{xx}}{\partial x} + \frac{\partial \sigma_{yx}}{\partial y} + b_x = 0, \quad \frac{\partial \sigma_{xy}}{\partial x} + \frac{\partial \sigma_{yy}}{\partial y} + b_y = 0 \tag{4}$$

subject to the boundary conditions $v_x=0$ and $v_y=0$ around the clamped rim of the plate. For a circular plate of radius a, we obtain the simplified expressions

$$v_x = \frac{\tau}{Eh}\frac{1-\nu^2}{3-\nu}(a^2 - x^2 - y^2), \quad v_y = 0 \tag{5}$$

and associated stresses

$$\sigma_{xx} = -\frac{2}{3-\nu}\frac{\tau}{h}x, \quad \sigma_{xy} = -\frac{1-\nu}{3-\nu}\frac{\tau}{h}y, \quad \sigma_{yy} = \nu\sigma_{xx} \tag{6}$$

These expressions confirm that the streamwise component of the in-plane normal stress, σ_{xx}, is positive (tensile) on the upstream half and negative (compressive) on the downstream half of the plate. The transverse component of the normal stress, σ_{yy}, is also positive or negative depending on the sign of the Poisson ratio. Compression raises the possibility of buckling and wrinkling when the shear stress τ exceeds a critical threshold.

To compute the transverse deflection along the z axis upon inception of buckling, $z=f(x,y)$, we work under the auspices of linear elastic stability of thin plates and shells and derive the linear von Kármán equation,

$$\nabla^4 f \equiv \nabla^2\nabla^2 f = \frac{\partial^4 f}{\partial x^4} + 2\frac{\partial^4 f}{\partial x^2 \partial y^2} + \frac{\partial^4 f}{\partial y^4} = \frac{h}{E_B}\left(\sigma_{xx}\frac{\partial^2 f}{\partial x^2} + 2\sigma_{xy}\frac{\partial^2 f}{\partial x \partial y} + \sigma_{yy}\frac{\partial^2 f}{\partial y^2} - b_x\frac{\partial f}{\partial x} - b_y\frac{\partial f}{\partial y}\right) - \frac{k}{E_B}f \tag{7}$$

where E_B is the bending modulus and k is the spring constant of the foundation with dimensions of force over cubed length (F/L^3). In a physiological context, the bending modulus of a typical biological membrane is $E_B \simeq 1\times 10^{-12}$ dyn·cm. In the human circulation, μ is on the order of 1 cP, or 1 mPa·s, and the shear stress varies in the range of 1–2 Pa through all branches, corresponding to $G \sim 100\ \mathrm{s}^{-1}$.

The fourth-order differential equation (Eq. (7)) incorporates position-dependent coefficients multiplying the second derivatives on the right-hand side. Since the membrane is assumed to be clamped around the rim, the deflection satisfies homogeneous Dirichlet and Neumann boundary conditions around the rim in the xy plane, $f=0$ and $\partial f/\partial n=0$, where $\partial/\partial n$ denotes the normal derivative.

Substituting the expressions for the in-plane shear stresses in Eq. (7) and nondimensionalizing lengths by the plate radius a, we derive the dimensionless parameters

$$\hat{\tau} = \frac{\tau a^3}{E_B}, \quad \gamma = \frac{k a^4}{E_B} \tag{8}$$

expressing, respectively, the strength of the shear flow and the stiffness of the spring relative to the developing bending moments. Equation (7) admits the trivial solution, $f=0$, for any value of $\hat{\tau}$ and nontrivial eigensolutions at a sequence of discrete eigenvalues. Numerical solutions for $\gamma=0$ were derived by Luo and Pozrikidis [5] using analytical and finite-element methods. The computation of these eigenvalues and corresponding eigenfunctions in the more general case where γ is nonzero is the main objective of our analysis.

When the plate is uniformly compressed, $\sigma_{xx}=-N/h$, $\sigma_{yy}=-N/h$, $\sigma_{xy}=0$, and $\sigma_{yx}=0$, and in the absence of a body force, the governing equation (Eq. (7)) reduces to

$$\nabla^4 f = -\frac{N}{E_B}\nabla^2 f - \frac{k}{E_B}f \tag{9}$$

where N is the magnitude of the isotropic compressive tension. Nondimensionalizing lengths by the plate radius a, we find that the solution depends on the dimensionless group $\Lambda \equiv Na^2/E_B$, and stiffness parameter γ. The eigensolutions of this equation were computed by Wang [3] for several types of boundary conditions using Fourier–Bessel expansions.

3 Fourier Series Solution

Following Luo and Pozrikids [5], we introduce the plane polar coordinates defined in Fig. 1 and nondimensionalize the position, radial distance, and membrane deflection by the patch radius a. Dimensionless variables are indicated by a hat; thus, $\hat{r}=r/a$ and $\hat{f}=f/a$. The eigenfunctions of Eq. (7) are expanded in Fourier series,

$$\hat{f}(\hat{r},\theta) = \frac{1}{2}p_0(\hat{r}) + \sum_{n=1}^{\infty}\left(p_n(\hat{r})\cos n\theta + q_n(\hat{r})\sin n\theta\right) = \sum_{n=-\infty}^{\infty} F_n(\hat{r})\exp(-in\theta) \tag{10}$$

where i is the imaginary unit, $p_n(\hat{r})$ and $q_n(\hat{r})$ are real functions, and $F_n(\hat{r})$ is a complex dimensionless function defined by

$$F_n(\hat{r}) \equiv \frac{1}{2}(p_n(\hat{r}) + iq_n(\hat{r})) \tag{11}$$

for $n \geqslant 0$. For $n<0$, $F_n(\hat{r}) = F^*_{-n}(\hat{r})$, where an asterisk denotes the complex conjugate. To ensure that the membrane shape is smooth at the origin, we require $F_n(0)=0$ for $n \geqslant 1$. A straightforward computation yields the following expressions for the Laplacian and bi-Laplacian in-plane polar coordinates:

$$\hat{\nabla}^2\hat{f} = \sum_{n=-\infty}^{\infty} Q_n(\hat{r})\exp(-in\theta), \quad \hat{\nabla}^4\hat{f} = \sum_{n=-\infty}^{\infty}\Omega_n(\hat{r})\exp(-in\theta) \tag{12}$$

where $\hat{\nabla}$ is the gradient with respect to $\hat{x}\equiv x/a$ and $\hat{y}\equiv y/a$,

$$Q_n \equiv F_n'' + \frac{F_n'}{\hat{r}} - n^2\frac{F_n}{\hat{r}^2} \tag{13}$$

a prime denotes a derivative with respect to $\hat{r}$, and

$$\Omega_n(\hat{r}) \equiv Q_n'' + \frac{Q_n'}{\hat{r}} - n^2\frac{Q_n}{\hat{r}^2} = F_n'''' + \frac{2}{\hat{r}}F_n''' - \frac{1+2n^2}{\hat{r}^2}F_n'' + \frac{1+2n^2}{\hat{r}^3}F_n' + n^2\frac{n^2-4}{\hat{r}^4}F_n \tag{14}$$

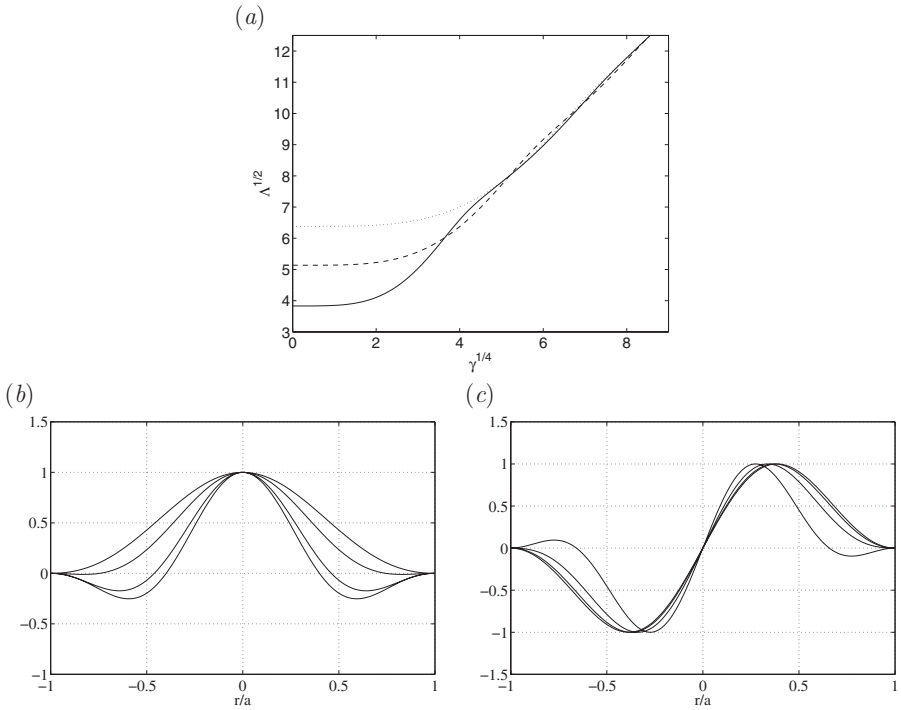

Fig. 2 (*a*) Effect of the elastic foundation constant γ on the lowest eigenvalues of a radially compressed circular plate for *n*=0 (solid line), *n*=1 (dashed line), and *n*=2 (dotted line). This figure reproduces Fig. 1 of Wang [3]. (*b*) and (*c*) Eigenfunctions, p_n, for $\gamma^{1/4}$=3, 4, 5, 6, and (*b*) *n*=0 and (*c*) *n*=1.

Expressing the right-hand side of Eq. (7) in plane polar coordinates and substituting the Fourier expansion, we find

$$\hat{\nabla}^4\hat{f} = -\sum_{n=-\infty}^{\infty}\left[\frac{\hat{\tau}}{3-\nu}\Psi_n e^{i\theta} + \gamma F_n + \frac{\hat{\tau}}{3-\nu}\Phi_n e^{-i\theta}\right]e^{-in\theta} \quad (15)$$

which can be restated as

$$\hat{\nabla}^4\hat{f} = -\sum_{n=-\infty}^{\infty}\left[\frac{\hat{\tau}}{3-\nu}\Psi_{n+1} + \gamma F_n + \frac{\hat{\tau}}{3-\nu}\Phi_{n-1}\right]e^{-in\theta} \quad (16)$$

where

$$\Psi_n = \hat{r}F_n'' + \left[\frac{3+\nu}{2} + (1-\nu)n\right]F_n' + n\left(\frac{1+\nu}{2} - \nu n\right)\frac{F_n}{\hat{r}}$$

$$\Phi_n = \hat{r}F_n'' + \left[\frac{3+\nu}{2} - (1-\nu)n\right]F_n' - n\left(\frac{1+\nu}{2} + \nu n\right)\frac{F_n}{\hat{r}} \quad (17)$$

Substituting Eq. (12) into Eq. (7) and equating corresponding Fourier coefficients, we derive an infinite tridiagonal system of ordinary differential equations,

$$\Omega_n + \gamma F_n = -\frac{\hat{\tau}}{3-\nu}(\Psi_{n+1} + \Phi_{n-1}) \quad (18)$$

for $n=0, \pm 1, \pm 2, \ldots$. Approximate eigenvalues are computed by truncating the system at a finite level, $n=\pm N$. In the case of eigensolutions with a left-to-right symmetry with respect to the zx plane, the Fourier series involves only cosine terms; the component functions F_n are real, $F_n=F_{-n}$, and $\Psi_{-n}=\Phi_n$. The general system (Eq. (18)) then reduces to

$$\Omega_0 + \gamma F_0 = -\frac{2\hat{\tau}}{3-\nu}\Psi_1$$

$$\Omega_n + \gamma F_n = -\frac{\hat{\tau}}{3-\nu}(\Psi_{n+1} + \Phi_{n-1}) \quad (19)$$

for $n=1,2,\ldots,N$. If the eigensolutions are antisymmetric with respect to the zx plane, the Fourier series involves only sine terms, the component functions F_n are imaginary, $F_n=-F_{-n}$, $\Psi_{-n}=-\Phi_n$, and the general system (Eq. (18)) reduces to $\Omega_0+\gamma F_0=0$ for the zeroth Fourier mode and the second equation in Eq. (19) for $n=1,2,\ldots,N$.

To solve the partial differential equations encapsulated in Eq. (18), we approximate the Fourier modulating modes $F_n(r)$ with polynomials, as discussed by Luo and Pozrikidis [5]. Collocating at Chebyshev nodes, we derive a generalized eigenvalue system of algebraic equations for the critical hydrodynamic stress. Physically, the smallest eigenvalue provides us with the minimum shear stress for the onset of buckling.

A similar method was implemented for solving Wang's compressed-plate equation (Eq. (9)). Substituting in Eq. (9) $\hat{f}(\hat{r},\theta)=p_n(\hat{r})\cos(n\theta)$, we derive the fourth-order ordinary differential equation

$$\mathcal{L}^2 p_n + \Lambda\mathcal{L}p_n + \gamma p_n = 0 \quad (20)$$

where

$$\mathcal{L} = \frac{d^2}{d\hat{r}^2} + \frac{1}{r}\frac{d}{d\hat{r}} - \frac{n^2}{r^2} \quad (21)$$

is a second-order differential operator. In this case, because of the uniform and isotropic tensions acting on the plate, the Fourier modes are decoupled.

4 Results and Discussion

To establish a point of reference, we first discuss the instability of the radially compressed plate governed by Eq. (20). Figure 2 demonstrates the effect of the elastic foundation parameter γ on

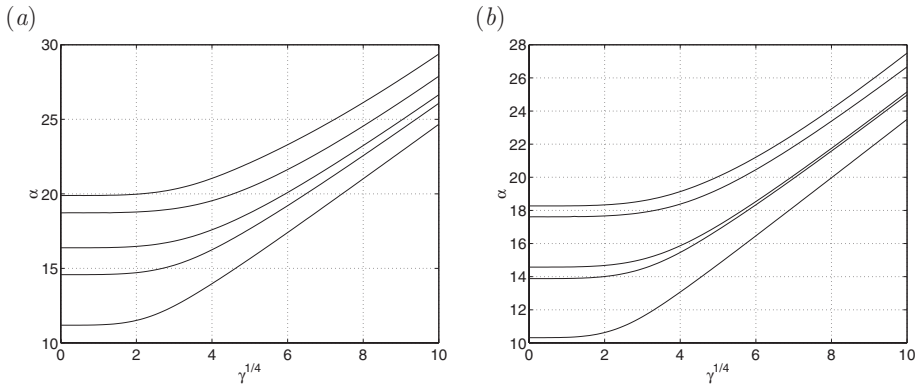

Fig. 3 Effect of the elastic foundation constant on the square root of the lowest eigenvalue, $\alpha=\sqrt{\hat{\tau}}$, for Poisson ratio (*a*) $\nu=0$ and (*b*) $\nu=0.25$. From bottom to top, the curves represent modes S1, S2, A1, A2, and S3, where "S" denotes a symmetric mode and "A" denotes an antisymmetric mode.

the lowest eigenvalues corresponding to $n=0$ (axisymmetric mode) and $n=1,2$ (nonaxisymmetric modes). The results precisely reproduce those shown in Fig. 1 of Wang [3] obtained by a different method. As γ is increased, the eigenvalue branches cross and then intertwine. Wang [3] noted that in the presence of a stiff elastic foundation, the axisymmetric mode is not necessarily the most dangerous buckling mode when the plate is strongly coupled to the foundation. As γ increases, the eigenfunctions of the axisymmetric mode and nonaxisymmetric modes take complicated shapes, as shown in Figs. 2(*b*) and 2(*c*).

Next, we discuss the instability of the circular plate under the action of a shear flow. Luo and Pozrikidis [5] found that, in the absence of the elastic substrate, $\gamma=0$, the buckling eigenfunctions consist of a sequence of symmetric modes, denoted as "S," interlaced with antisymmetric modes, denoted as "A." Figure 3 shows the effect of the substrate elastic parameter γ on the lowest few eigenvalues $\hat{\tau}$ for $\nu=0$ and 0.25. As γ increases, the eigenvalues increase monotonically while maintaining their relative position. In contrast to the radially compressed plate, the buckling modes caused by the hydrodynamic shear stress do not cross, and the symmetric mode S1 is always the most dangerous buckling mode. Selected eigenfunctions for $\nu=0.25$ and $\gamma=625$ are shown in Fig. 4.

Figure 5 illustrates the effect of γ on the profile of the eigenfunctions in the zx plane for the symmetric eigenmodes corresponding to $\nu=0.25$ and $\gamma=0$, 625, and 6561. For high values of γ, the buckled shape is convoluted even for the lowest mode. As γ increases, the deflection becomes more pronounced at the downstream portion of the plate.

Luo and Pozrikidis [5] found that the Poisson ratio may affect the order of appearance of the symmetric and antisymmetric eigenmodes, as illustrated in Fig. 6 for $\gamma=0$, 625, and 4096. In all cases, the eigenvalue $\hat{\tau}$ decreases as ν is increased, and the rate of decrease varies for each eigenmode. At certain critical Poisson ratios, the pair of the S2 and A1 modes and the pair of the S3 and

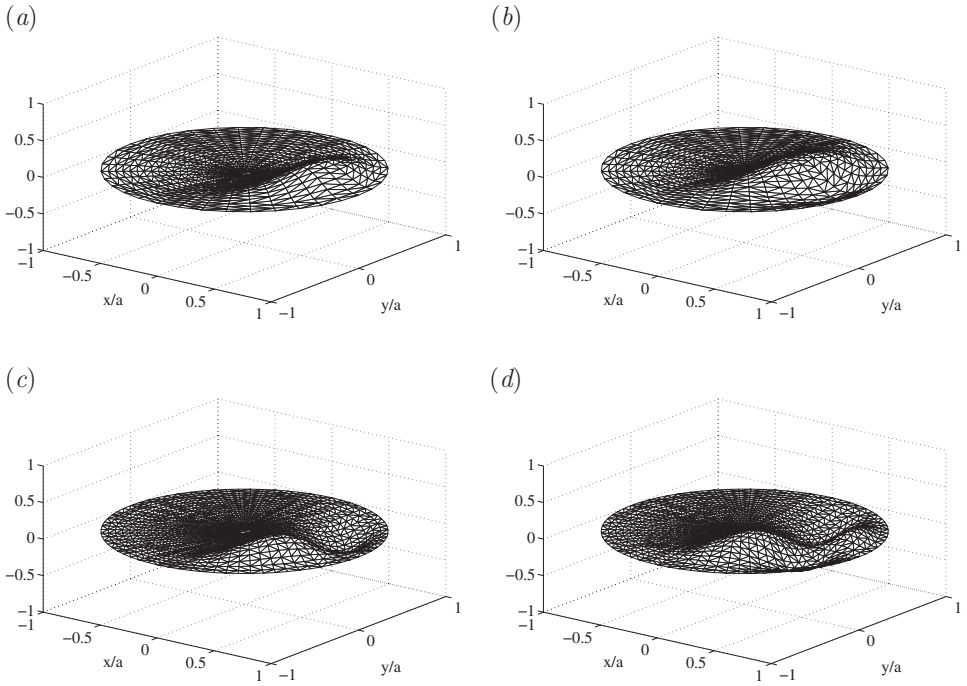

Fig. 4 Buckling eigenmodes for $\nu=0.25$, $\gamma=625$, and (*a*) $\hat{\tau}=217.24$ (S1), (*b*) $\hat{\tau}=282.93$ (S2), (*c*) $\hat{\tau}=291.82$ (A1), and (*d*) $\hat{\tau}=371.08$ (A2)

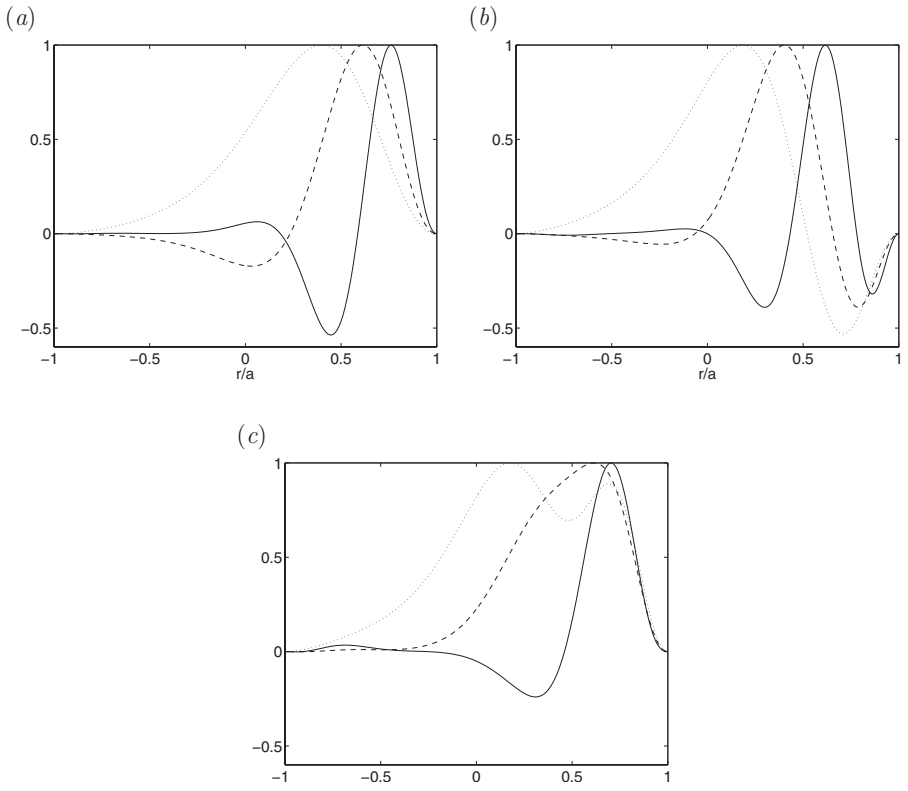

Fig. 5 Comparison of the buckling mode profiles for ν=0.25 and γ=0 (dash-dotted line), γ=625 (dashed line), and γ=6561 (solid line), and buckling modes (*a*) S1, (*b*) S2, and (*c*) S3

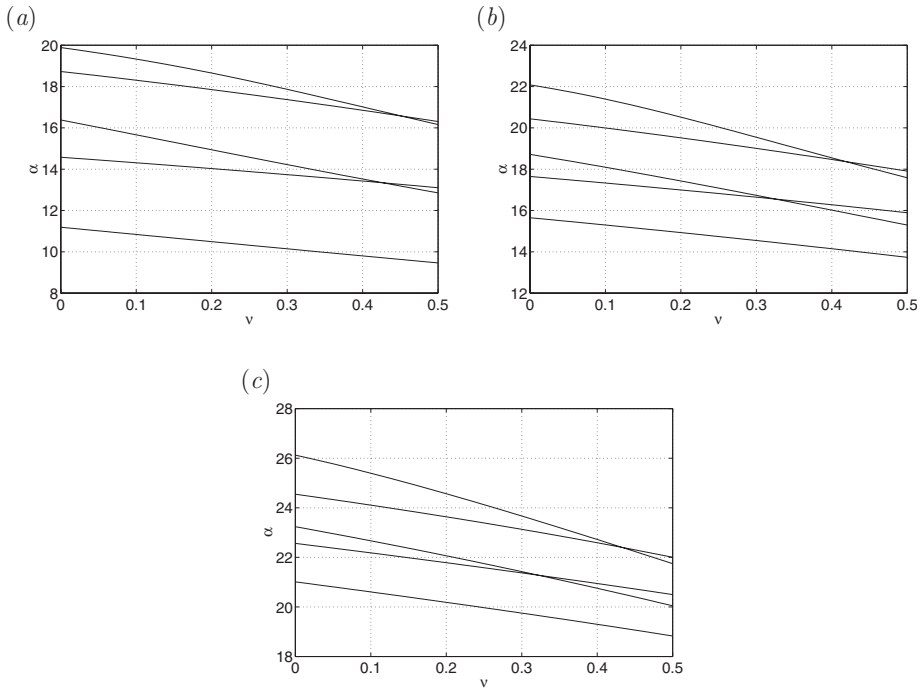

Fig. 6 First few eigenvalues, $\alpha=\sqrt{\hat{\tau}}$, plotted against ν for a circular membrane with the spring stiffness (*a*) γ=0, (*b*) γ=625, and (*c*) γ=4096. From bottom to top along ν=0, the curves represent modes S1, S2, A1, A2, and S3.

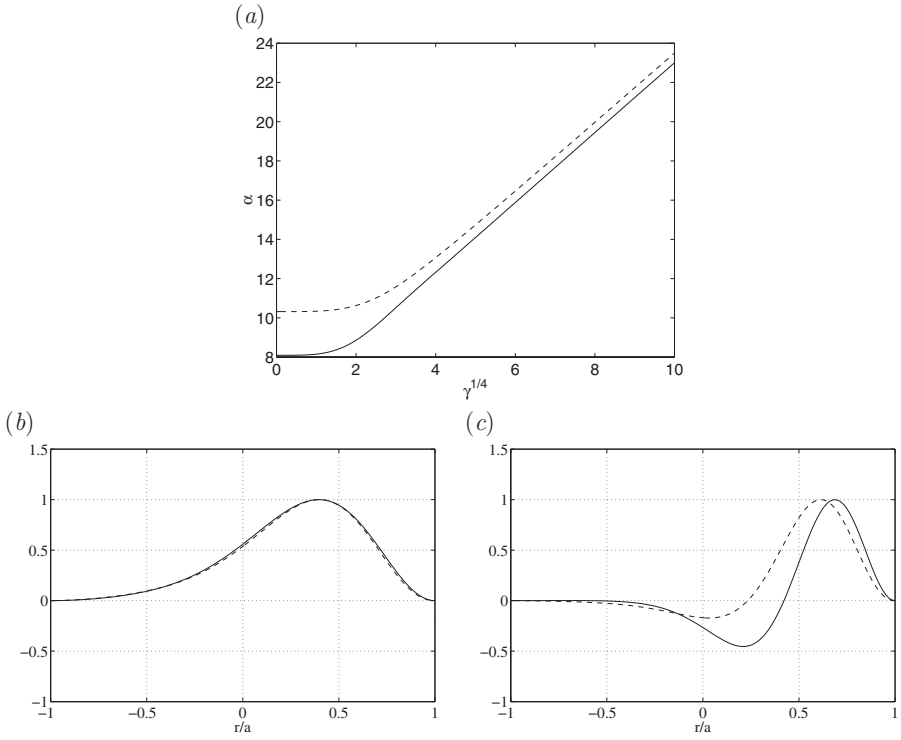

Fig. 7 (*a*) The lowest eigenvalues of the one-dimensional model, $\alpha=\sqrt{\hat{\tau}}$ (solid line), are compared with the S1 eigenvalues of the two-dimensional model (dashed line). (*b*) and (*c*) The solid lines illustrate the eigenfunctions of the one-dimensional model for (*b*) $\gamma=0$ and (*c*) $\gamma=625$. The profiles of the two-dimensional eigenfunction S1 at $y=0$ are shown as dashed lines.

A2 modes cross over. At these Poisson ratios, the eigenfunctions of the double eigenvalues are arbitrary superposition of the symmetric and antisymmetric modes and may thus have an arbitrary orientation in space. The critical Poisson ratios are affected only slightly by γ.

It is instructive to compare the numerical results of the full two-dimensional model with the predictions of a one-dimensional model that arises by applying the von Kármán equation at the midplane, $y=0$, and discarding the y dependence. The deflection is governed by a linear ordinary differential equation with position-dependent coefficients,

$$\frac{d^4f}{dx^4}+\frac{k}{E_B}f=-\frac{2\tau}{(3-\nu)E_B}\left(x\frac{d^2f}{dx^2}+\frac{3-\nu}{2}\frac{df}{dx}\right) \tag{22}$$

subject to the clamped-end boundary conditions $f=0$ and $f'=0$ at $x=\pm a$. The nondimensional form is

$$\frac{d^4\hat{f}}{d\hat{x}^4}+\gamma\hat{f}=-\frac{2\hat{\tau}}{3-\nu}\left(\hat{x}\frac{d^2\hat{f}}{d\hat{x}^2}+\frac{3-\nu}{2}\frac{d\hat{f}}{d\hat{x}}\right) \tag{23}$$

On physical grounds, we anticipate that the eigenvalues and corresponding eigenfunctions will be approximations of the symmetric circular membrane modes.

We were unable to solve the one-dimensional eigenvalue problem by analytical methods. Numerical solutions were produced instead using a finite-difference method resulting in a pentadiagonal system of algebraic equations for the nodal values of the eigenfunctions. Figure 7(*a*) compares the eigenvalues of the one-dimensional model with the S1 eigenvalues of the two-dimensional model. The critical buckling load predicted by the one-dimensional model is lower than that of the two-dimensional model and thus provides us a conservative prediction independent of the elastic foundation constant. Figures 7(*b*) and 7(*c*) compare the first buckling mode of the one-dimensional model for $\gamma=0$ and $\gamma=625$ with the corresponding eigenfunction profiles of the two-dimensional solution at $y=0$. The agreement is excellent for $\gamma=0$ and reasonable for $\gamma=625$. We conclude that the one-dimensional model is useful for making reliable engineering predictions.

5 Conclusion

We have investigated the effect of an elastic foundation on the buckling of a circular plate under the action of a uniform body force tangential to the plate, imparted by an overpassing simple shear flow. In the case of the radially compressed circular plate, a nonaxisymmetric deflection in an indeterminate meridional position may occur when the plate-substrate coupling is sufficiently strong. Buckling first occurs in the symmetric mode where the deflection is left-to-right symmetric with respect to the direction of the flow. Our results serve as a guide for future laboratory observations aimed at documenting the buckling of exposed cells and assessing their significance in mechanotransduction.

Acknowledgment

This research was supported by a grant provided by the National Science Foundation.

References

[1] Bloom, F., and Coffin, D., 2001, *Handbook of Thin Plate Buckling and Postbuckling*, Chapman and Hall/CRC, Boca Raton.
[2] Timoshenko, S. P., and Gere., J. M., 1961, *Theory of Elastic Stability*, 2nd ed., McGraw-Hill, New York.
[3] Wang, C. W., 2005, "On the Buckling of a Circular Plate on an Elastic Foundation," ASME J. Appl. Mech., **72**, pp. 795–796.
[4] Fung, Y. C., and Liu, S. Q., 1993, "Elementary Mechanics of the Endothelium of Blood Vessels," ASME J. Biomech. Eng., **115**, pp. 1–12.
[5] Luo, H., and Pozrikidis, C., 2006, "Buckling of a Flush Mounted Plate in Simple Shear Flow," Arch. Appl. Mech., **76**, pp. 549–566.
[6] Luo, H., and Pozrikidis, C., 2007, "Buckling of a Pre-Compressed or Pre-Stretched Membrane in Shear Flow," Int. J. Solids Struct., 44, pp. 8074–8085.